HISTORICAL SEISMOLOGIST

Quantifying Earthquake Effects on Ancient Arches, Example: The Kalat Nimrod Fortress, Dead Sea Fault Zone

by Klaus-G. Hinzen, Iris Schwellenbach, Gregor Schweppe, and Shmuel Marco

ABSTRACT

Deformed arches are often key elements of archaeoseismic studies; arches have been in use for more than three millennia and damage, particularly moved keystones, are clear indications of a seismogenic cause. We introduce a damage evaluation scheme that allows a straightforward determination of the degree of damage to an arch based on laser scan models and digital images. The scheme is applied to 90 arches of the Nimrod Castle, which is neighboring the Dead Sea fault and which was heavily damaged during the 1759 Lebanon earthquake. The analysis shows that the *a priori* assumption of a correlation between arch orientation and damage degree does not hold for the entire building. An exception is a large tower including a secret passage in which voussoirs have dropped along a more than 20 m long section.

INTRODUCTION

Earthquake effects on archaeological structures and the environment can take on various forms of appearance (Marco, 2008). Rodríguez-Pascua *et al.* (2011) suggested a scheme to categorize what they called Earthquake Archaeological Effects (EAEs) into (1) geologic effects, (2) building effects (both of which are considered as primary effects), and (3) secondary effects such as fire, abandonment of sites, etc. Although this scheme provides a method of systematically identifying and categorizing the EAEs when exploring an excavated site or evaluating a persisting monument, it does not include any quantification of the severity of the observed effects. However, the latter is essential if reasonable interpretations of the causative seismic ground motions are of interest or damage patterns are to be made.

Among the "building fabric effects", which following Rodríguez-Pascua *et al.* (2011) are a sign of strain deformational features generated by transient shaking, the sixth EAE listed in their table is that of "Dropped key stones in arches or lintels in windows and doors." In this contribution, we concentrate on the EAEs on stone arches, which in addition to the drop of keystones can include several other forms of deformations, such as rotation, and/or cracking and spalling.

Arches represent an important building element in archaeoseismology for several reasons: (1) arches have been in use for some 4000 years, (2) arches are found in many cultural backgrounds, and most importantly, (3) although many EAEs may have causes other than earthquake ground motions, a drop of keystones or voussoirs of arches is only possible in cases of destabilization of the static situation. This induced instability, in turn, can only be caused by a transient (horizontal) ground motion, usually parallel to the trend of the arch, unless compression failure of blocks occurs due to alteration.

Several approaches have been made to study the behavior of arches under dynamic loading, both analytically and numerically, as well as with small scale models (e.g., Fanning *et al.*, 2001; De Lorenzis *et al.*, 2007; Kamai and Hatzor, 2007; De Jong, 2012; De Jong and Vibert, 2012). To compare modeling results and observations, a systematic approach to describing the damage—as is suggested in this contribution—is helpful.

Structures or archaeological sites with a large number of arches oriented in different directions are interesting archaeoseismological targets. The main questions to be answered for such sites are: (1) is the orientation of strain uniform within a large structure; (2) is the strain orientation in the arches indicative of an earthquake source; and (3) what determines the type and degree of damage in individual arches, is it the wall orientation, the shape/geometry of the arch, or the location within the site?

FEATURES OF ARCHES

Arches (Fig. 1) are pure compression construction forms and help to span wall openings by diverting vertical loads from above to compressive stress (Dym and Williams, 2011). They make use of the fact that natural building materials possess a high compressive strength compared to their low tensile strength. The forces in the arch are carried to the ground and

doi: 10.1785/0220150282

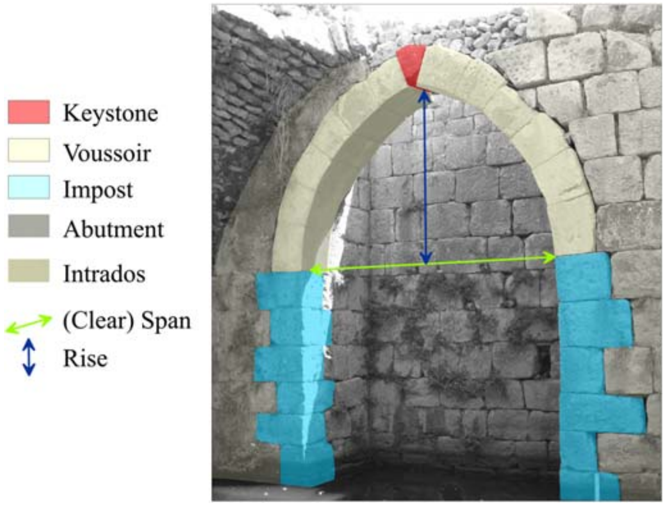

▲ **Figure 1.** Elements and dimensions of a stone arch overlain on a photograph of arch number A6.2 from Table 1 located on the eastern side of the large cistern of Kalat Nimrod Fortress. The color version of this figure is available only in the electronic edition.

are proportional to the span and inversely proportional to the rise (Fig. 1). Increasing load will cause an increase of the outward push at the arches' base, referred to as an "arches' thrust" (Fig. 2) (Ambrose and Tripeny, 2011). To make the arch stable, the thrust must be restrained by either internal ties (e.g., clamping devices) or by external bracing through appropriate buttresses.

Figure 1 shows the common nomenclature used for the individual parts forming an arch and its major dimensions. Arches of various types have been in use at least since the Bronze Age. Early versions, for example, in Mycenaean structures, were corbeled arches where the wall gap is being closed by successively offsetting stone courses from the sides until they meet in the center and the top is closed by a flagstone (Fig. 2). Corbeled arches are not considered true arches, as not all of the tensile stresses from the weight of the superstructure are transformed to compressive stresses in the blocks forming the arch, and consequently corbeled arches are not completely self-supporting structures.

The Ashkalon arch in Israel, dating to 1850 BCE, is by some sources considered to be the oldest true arch known (Schloen, 1995). The ancient Greeks developed arch engineering and the Romans adopted the techniques from the Etruscans. In the first century CE, the Romans extended the arch building technique to vaults that could roof large interior spaces.

DAMAGE QUANTIFICATION SCHEME

To define a quantification scheme of the damage to arches, we followed the approach of damage grades to structures given in the European Macroseismic Scale EMS98 (Grünthal, 1998). Our definition of arch damage grade (ADG) is based on three categories: (1) fractures of plaster and/or mortar (if any) and fracturing of the building blocks of the arch, (2) deformations, including vertical and horizontal movements of voussoirs and/or keystones including rotations, and (3) spall and breakout, particularly at the corners of pillar stones, voussoirs, and keystone. Figure 3 shows examples of damage for these categories of differing severity.

The importance of the amount of movement of individual blocks of arches from their original position varies with the overall size of the structures. Therefore, we related the horizontal and vertical components of movement of blocks to the span and the rise of the arches, respectively. Damage grades were assigned to the percentage bins of these movement measures listed in Figure 4. The bins are somewhat arbitrary; however, we tried to adhere to the accuracy with which the deformations can be measured and also utilized our experience from inspecting numerous arches at different archaeological sites. For fractures and spall, we followed a more descriptive approach similar to that used in intensity scales. The definitions of quantities (few, many, most) are adopted from the EMS98.

Figure 4 shows a spreadsheet that allows a rapid estimate of the overall ADG by clicking the appropriate radio button in each category. In general, the average of the individual grades from all categories is taken as the total ADG. Exceptions to this are only made when the keystone and one or more voussoirs dropped; in this case, the grade is set to 7, independent of the grades in other categories. In case of a collapsed arch, ADG 8 is assigned.

This scheme was developed mainly for application to round or segmental arches. An original draft of the scheme was modified and adapted during the processing of the 95 arches used as examples in this study. The form of an arch has a significant influence on how it reacts to ground motions. For Lancet or equilateral pointed arches that do not have a classical keystone, a somewhat modified scheme would be necessary to deduce ADGs.

THE NIMROD CASTLE

Kalat Nimrod (originally called Kalat Subayba) overlooks a narrow, deep valley that separates Mount Hermon from the rest of the Golan Heights. It was built during the thirteenth century starting in 1228 to control the road linking the Galilee with Damascus, and the former Crusader town of Banias (Ellenblum, 1989). The fortress complex (Fig. 5) extends 420 m east–west and 150 m north–south. It was built of large, squared ashlars. Along the walls are numerous semicircular and rectangular towers. These are roofed with pointed cross arches. At the eastern edge of the fortress stood a large keep, measuring 65 × 45 m and protected by massive rectangular towers.

Geologic Setting

The hill of Kalat Nimrod (Fig. 5) consists of early Jusassic limestone, the same formation that comprises most of Mount Hermon (Sneh and Weinberger, 2003). Mount Hermon forms part of a northeast-trending anticlinal structure that was formed by superposition of two tectonic stages: the anticlinal folding that is part of the Cretaceous to the Early Tertiary "Syrian Arc" fold belt, and a right (restraining) bend of the sinistral Dead Sea fault (DSF) system (Garfunkel, 1981). The

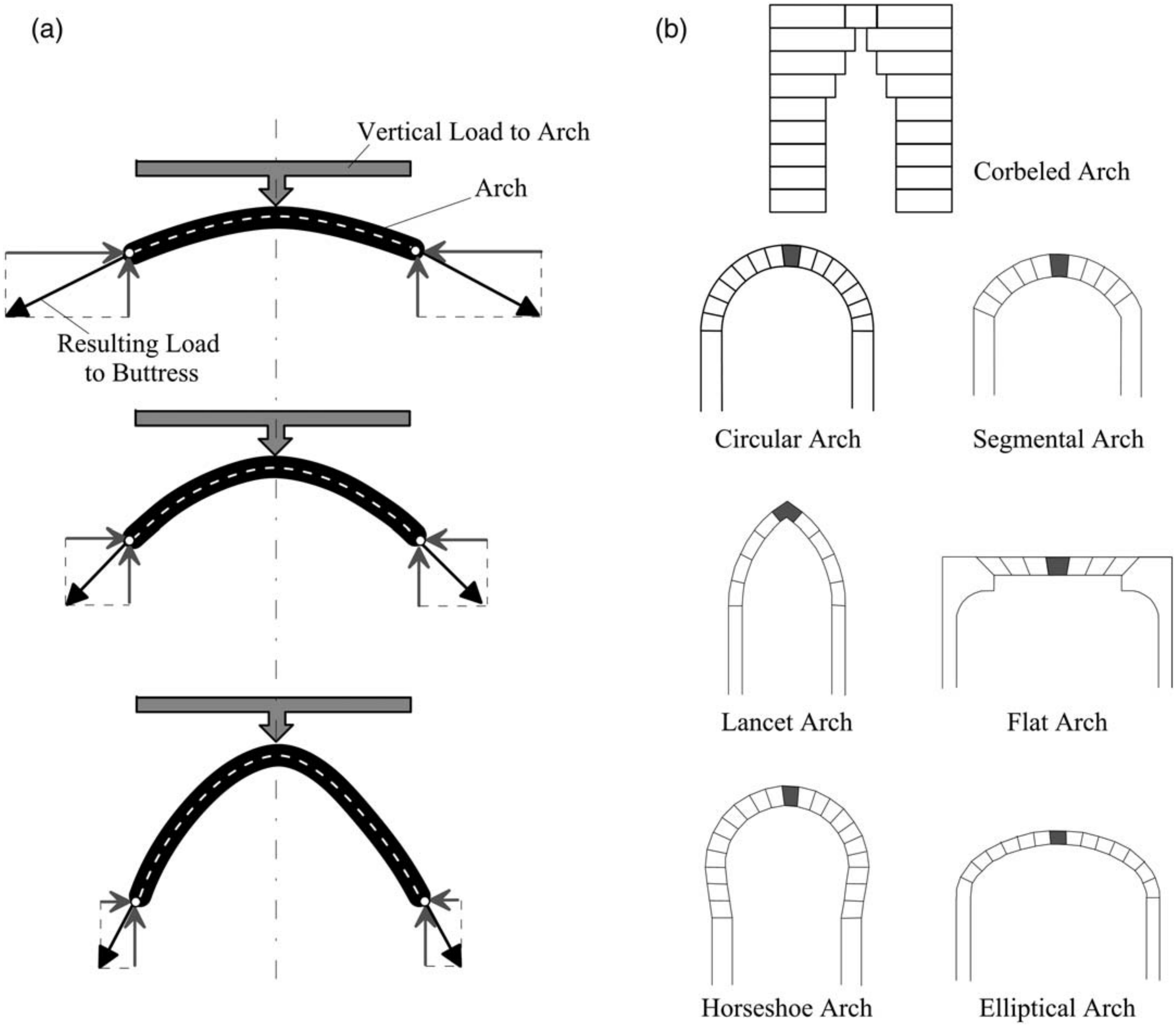

▲ **Figure 2.** (a) Top to bottom, three arches of similar span, but different rise with schematically shown forces to the buttresses. (b) Principle structure of a corbeled arch and six types of true arches. Keystones are shown in gray (after Ching, 2014).

fortress is built on top of a dominant hill between elevations of 770 m at the western end and 830 m at the eastern end (33°15′ 9.52″N; 35°42′54.24″E). Early Cretaceous mafic dikes, lavas, and pyroclastics that had intruded into the Jurassic sediments (Wilson *et al.*, 2000) were interpreted as part of a hot spot trace in the Middle East (Garfunkel, 1991).

The DSF branches into three strike-slip faults at the northern end of the Hula Valley: the Serghaya, Rachaya, and Hasbaya faults, along with the main carrier of the motion which is on the Yammouneh fault (Garfunkel *et al.*, 1981). Paleomagnetic records that show counter-clockwise rotations of up to 65° in the vicinity of Mt. Hermon indicate that this geometry of left-lateral strike-slip faults is associated with rotations of the intervening blocks as a mechanism for partial accommodation of transpression within the restraining bend of the DSF (Ron, 1987). The Nimrod fortress is built on a block that is bounded by the Rachaya fault on the northwest and a complex fault zone on the southeast (Fig. 5c).

Seismicity

The historical earthquakes that postdate the construction of the fortress occurred in November 1759 and in January 1837. The latter one, which was attributed to surface rupture along the Roum fault (Nemer and Meghraoui, 2006), primarily affected southern Lebanon (Ambraseys, 1997). In a detailed account by George Robinson, who traveled in the Middle East in 1837 shortly after the earthquake, the fortress is described as having suffered damage by an ancient earthquake (Robinson,

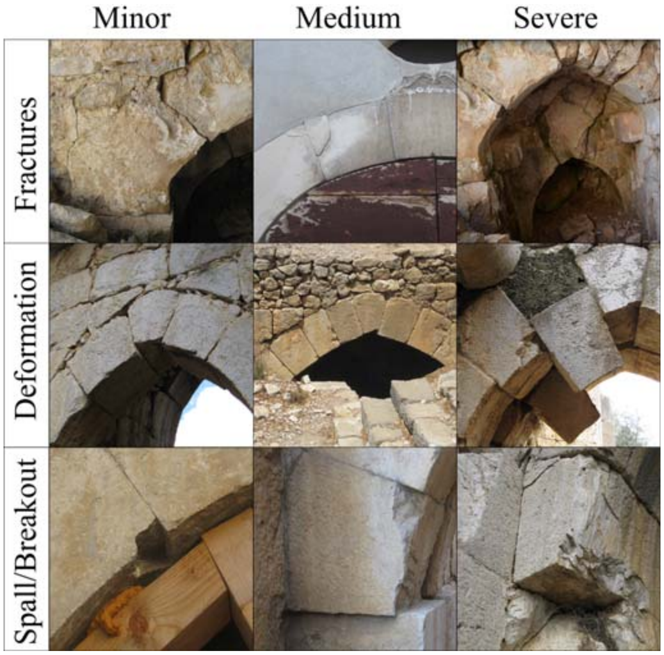

▲ **Figure 3.** The matrix shows photos of examples of damage to stone arches. Rows correspond to the indicated damage category and columns to the severity of the damage. The color version of this figure is available only in the electronic edition.

1837). We therefore assume that the 25 November 1759 earthquake caused most of the observed damage. The source of this earthquake along the Serghaya fault is determined by paleoseismic studies (Gomez *et al.*, 2001; Nemer *et al.*, 2008). This determination conforms with the center of damage delineated by Sieberg (1932) and Ambraseys and Barazangi (1989). The rupture of an earlier earthquake that occurred in 30 October 1759 offset archaeological structures of Tell Ateret (Marco *et al.*, 1997; Ellenblum *et al.*, 2015) and a series of streams (Marco *et al.*, 2005) along the Jordan Gorge section of the DSF. However, the measured slip of 0.5 m indicates a moderate earthquake with an estimated magnitude of ~6.2 based on the extent of damage and contemporary reports (Ambraseys and Barazangi, 1989). We cannot rule out that some of the damage to the fortress was associated with the 30 October 1759, but it is unlikely that it was extensive.

3D Laser Scans and Damage Analysis

The semicircular arches, on which we concentrate in this study, became a popular feature in Islamic sacral, as well as defense, architecture. It was probably adopted from horseshoe arches which were constructed as early as the fifth century by Persians and Byzantines in Syria and Persia.

A contemporary visitor usually enters the remains of Kalat Nimrod from the southwest. The most striking features here are the walls of the gate tower (Hartal, 2001). From the platform, which was once the first floor of the extended tower, completely surrounded by walls and now in the open, one can see the most spectacular damage: the two arches oriented east–west (the severe deformation photo in Fig. 3) with the eastern voussoir next to the keystone moved by up to 26% of the rise, whereas the neighboring arches at 2 m distance in north–south orientation do not show severe deformation. Although exploring the rest of the fortification, the impression may arise that directionality in the overall damage pattern of the arches exists. So quantification of ADG was used to test this subjective impression.

To systematically study the state of the arches of Kalat Nimrod, we used digital images and 3D laser scans. The latter were taken by a high-resolution phase scanner which allows quick (up to 900, 000 pts/s) and 3D surveying of the targets. Depending on the scan targets, at least two but sometimes up to six, single scans were combined to a 3D model of the targeted arch. Table 1 lists the 95 arches which were accessible and selected for this study. In addition to the location in a local rectangular coordinate system (Fig. 6), the azimuth with respect to north and the dimensions are listed.

Earthquake Archaeological Effects (EAE)
Arch Damage Grade (ADG)

Arches

		Deformation				
		Vertical		Horizontal		
Grade	Fractures	Voussoirs	Key Stone	In Plane	Out of Plane	Spall
8	○ collapsed					
7	○ crushed blocks	○ drop	○ drop			
6	○ broken blocks	◉ d > 10% of rise	○ d > 10% of rise	◉ d > 5% of span	○ > 5% of span	◉ large patches at many corners
5	○ fractures in most blocks	○ 5 < d < 10% of rise	◉ 5 < d < 10% of rise	○ 3 < d < 5% of span	○ 3 < d < 5% of span	○ large patches at few corners
4	○ extended fractures in many blocks	○ 2 < d < 5% of rise	○ 2 < d < 5% of rise	○ 2 < d < 3% of	◉ 2 < d < 3% of span	○ small patches at many corners
3	○ extended fractures in few blocks	○ 1 < d < 2% of rise	○ 1 < d < 2% of rise	○ 1 < d < 2% of span	○ 1 < d < 2% of span	○ small patches at few corners
2	◉ small fractures in few blocks	○ d < 1% of rise	○ d < 1% of rise	○ d < 1% of span	○ d < 1% of span	○ minor patches at single/few corners
1	○ only in plaster or mortar	○ none	○ none	○ none	○ none	○ none

ADG: 5.5

▲ **Figure 4.** Spreadsheet which allows a rapid estimate of the arches damage grade (ADG) by simply clicking the appropriate radio button in each category. The resulting ADG in this example is 4.3. The color version of this figure is available only in the electronic edition.

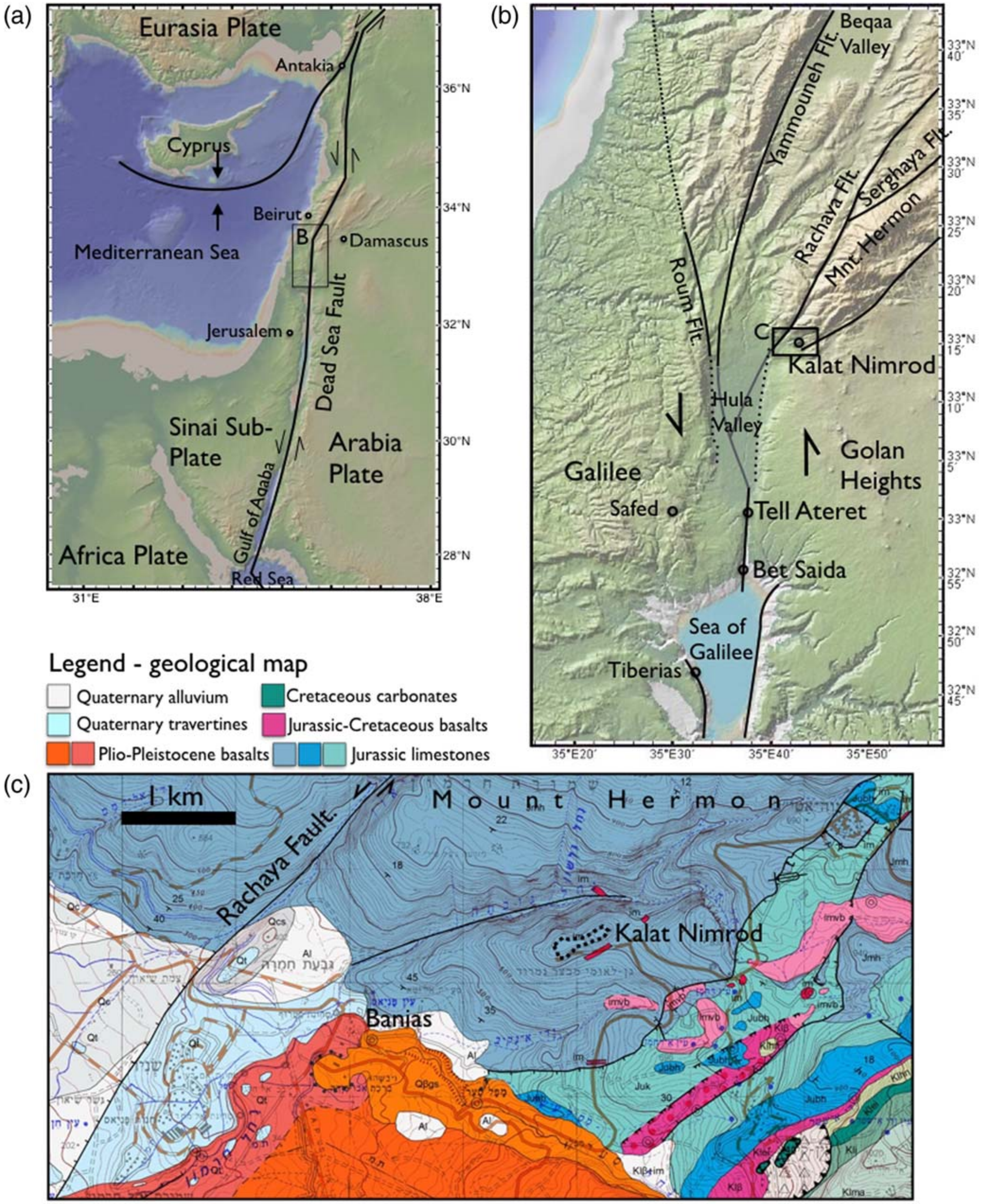

▲ **Figure 5.** Location map of the Kalat Nimrod castle on the Golan Heights. (a) Dead Sea fault and surroundings, the rectangle indicates the location of the more detailed map in (b). Local geology and faults neighboring Kalat Nimrod are shown in panel (c), after Sneh and Weinberger (2014). The color version of this figure is available only in the electronic edition.

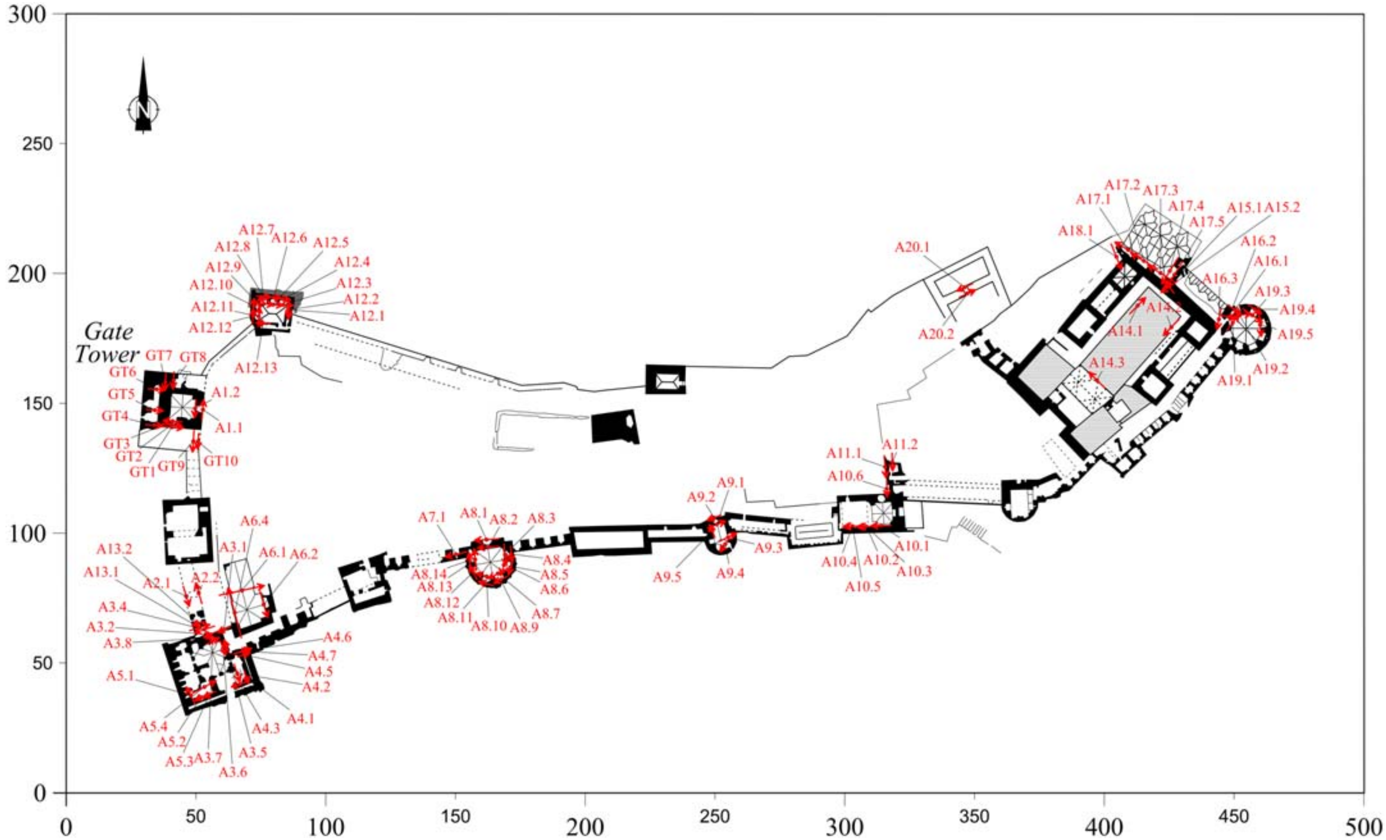

▲ **Figure 6.** Plan of the Kalat Nimrod castle based on the work of Deschamps (1939) and Hartal (2001). Superimposed on the major structural elements of the fortification are the 95 arches listed in Table 1. The center of each arrow represents the position of an arch, the arrow head points to the right when looking at the arch from the outside, and the arrow length varies with the span of the arch. Labels are those from Table 1. The axis units are in meters, the origin of the local coordinate system was chosen at the southwestern corner of the fortress. The color version of this figure is available only in the electronic edition.

Figure 7 summarizes the basic measurements of the sizes and orientations of the 95 arches from Table 1. The rise of most arches follows a clear linear relation of 0.55 times the span, indicating that the arch type is circular (Fig. 2b).

For the analysis of an individual arch, a plot with the digital photograph next to an orthographic front view from the laser scan, a crosscut view and a longitudinal section were produced (Fig. 8). Displacement vectors were measured within the scan model and cracks and breakouts marked on the photos. These plots, in combination with the deformation measures, were used to fill out the evaluation sheet from Figure 4 for each arch.

Of the 95 arches, ADGs were determined for 90; the view to the missing five was obscured so that not all the important parts of the arches were visible. The histogram in Figure 8e shows that the ADGs range from 1 to 8, with a maximum of the distribution between ADGs of 3 to 3.5. A slight tendency toward increased ADGs with increasing arch span might be deduced from Figure 8f; however, there are not enough wide arches with a span above 4 m to adequately quantify this conclusion. Figure 8g shows that the original hypothesis of a clear correlation between the azimuthal orientation of an arch and the damage it suffered does not hold. Considering the fact that there are only few arches within the azimuthal ranges from 20° to 50° and 125° to 140° the distribution of ADGs with azimuth appears to be fairly uniform. The spatial distribution of ADGs is plotted on top of the plan of Kalat Nimrod in Figure 9.

The Secret Passage

The gate tower that was built in 1230 (Fig. 6) (Hartal, 2001) was partially destroyed during the 25 November 1759 Lebanon earthquake. A wedge extending from the western base to the eastern top of the tower collapsed and the remains are found at the foot of the hill. However, the eastern elements of the tower survived intact and display interesting deformations, including those in a so-called secret passageway which filled the space between the tower's western wall and the cliff. At the time when the fortification was damaged by the earthquake, the gate tower had been significantly extended compared with its original size. Hartal (2001) reconstructed the size at the base of the extended tower to 22.5 × 31.8 m and a height of more than 30 m. The extension, when intact, was mantling the former tower on all but the eastern side where the lower part of the tower is leaning against the outcropping bedrock. The passage has a total length of 27 m, is 1.80 m wide and includes an upper

Table 1
Code Name, Location, Size, and Damage Grade for Arches at the Kalat Nimrod Fortress

	Location							
Code	***X***	***Y***	**Azimuth**	**Number of Voissoirs**	**Span (m)**	**Rise (m)**	**Pier Height (m)**	**ADG**
A1.1	52.65	147.57	−5	8	2.30	1.47	3.05	2.8
A1.2	49.73	147.96	175	6	1.97	0.98	2.67	3.4
A2.1	46.30	75.67	197	8	2.53	1.14	1.33	3.1
A2.2	51.08	76.86	17	8	2.64	1.16	1.28	3.1
A3.1	60.86	62.84	114	4	1.15	0.71	1.50	4.0
A3.2	55.55	60.99	114	4	1.17	0.73	1.61	3.4
A3.4	53.31	62.84	109	10	2.61	1.27	4.24	2.3
A3.5	61.77	56.36	22	4	1.05	0.67	1.70	2.6
A3.6	60.45	55.70	202	8	1.31	0.84	2.07	2.3
A3.7	56.49	58.47	−63	4	1.26	0.66	2.01	3.5
A3.8	55.30	59.54	27	4	1.02	0.66	3.13	1.3
A4.1	69.44	44.48	199	4	0.90	0.51	1.51	4.4
A4.2	65.86	46.05	198	8	2.06	1.32	1.52	3.6
A4.3	67.06	41.83	108	8	2.03	0.87	1.99	2.0
A4.4	67.06	41.83	108	6	1.30	0.86	NA	2.1
A4.5	68.50	53.19	288	4	0.88	0.52	1.52	2.3
A4.6	68.00	54.51	286	4	1.03	0.65	1.00	2.3
A4.7	68.00	54.51	−73	8	2.15	1.40	1.50	3.0
A4.8	68.00	54.51	−73	6	1.40	0.81	1.49	3.8
A5.1	48.01	37.47	27	8	2.12	1.20	1.54	3.1
A5.2	51.89	36.70	118	10	0.88	0.63	0.99	3.1
A5.3	55.17	37.80	118	7	0.94	1.03	0.90	3.0
A5.4	53.29	40.74	298	12	3.80	2.30	1.53	2.3
A6.1	67.72	77.90	282	32	8.12	4.60	NA	3.6
A6.2	76.17	72.49	196	12	4.00	2.65	6.16	3.0
A6.4	64.95	69.32	15	16	9.40	4.80	1.47	—
A7.1	150.22	91.80	104	10	2.82	1.82	0.59	3.1
A8.1	161.98	97.46	94	10	3.30	2.20	1.99	1.6
A8.2	162.64	94.56	94	4	2.64	0.61	2.10	1.8
A8.3	169.11	91.64	185	8	2.71	1.75	1.57	2.3
A8.4	171.48	91.92	185	5	1.38	0.82	1.52	2.0
A8.5	168.71	87.68	162	8	2.74	1.74	1.50	2.8
A8.6	171.35	86.77	162	4	1.37	0.86	NA	1.9
A8.7	166.32	84.38	118	8	2.74	1.69	1.46	1.9
A8.9	167.39	82.02	118	6	1.36	0.81	1.66	2.0
A8.10	161.98	83.34	74	8	2.77	1.71	1.43	2.1
A8.11	161.70	80.54	74	6	1.37	0.83	1.59	2.0
A8.12	156.82	84.91	29	6	1.42	0.82	1.10	3.5
A8.13	157.61	89.81	6	8	2.72	1.72	1.46	1.9
A8.14	155.50	89.54	6	4	1.34	0.81	1.65	3.9
A8.15	155.50	89.54	29	3	2.71	NA	1.04	8.0
A9.1	250.67	103.28	−69	4	2.18	0.85	2.15	2.1
A9.2	249.61	105.92	111	4	1.21	0.73	1.64	2.8
A9.3	255.02	98.40	−64	6	2.21	1.48	1.67	2.6

Arch damage grade (ADG).
(Continued next page.)

Table 1 (continued)
Code Name, Location, Size, and Damage Grade for Arches at the Kalat Nimrod Fortress

Code	Location X	Location Y	Azimuth	Number of Voissoirs	Span (m)	Rise (m)	Pier Height (m)	ADG
A9.4	253.98	95.76	146	6	2.12	1.33	1.68	2.3
A9.5	248.95	100.79	23	4	1.03	0.65	1.67	3.1
A10.1	313.97	102.90	91	4	2.28	0.66	1.42	3.4
A10.2	308.31	102.49	92	4	2.24	0.63	1.55	3.6
A10.3	308.31	102.49	92	6	1.26	0.81	1.47	4.5
A10.4	303.00	102.62	92	4	2.21	0.62	1.64	5.5
A10.5	303.00	102.62	92	6	1.59	0.87	1.37	4.1
A10.6	316.23	117.04	181	5	1.58	1.15	NA	4.8
A11.1	315.57	125.50	185	10?	2.84	1.56	NA	6.0
A11.2	318.34	127.36	182	6	1.87	0.94	NA	—
A12.1	85.83	186.03	177	8	2.25	1.02	1.93	3.9
A12.2	85.83	186.03	177	4	1.26	0.77	1.52	4.9
A12.3	83.72	187.88	266	8	2.36	1.50	1.49	3.5
A12.4	83.59	190.12	266	4	1.22	0.82	1.54	2.9
A12.5	79.76	188.01	266	8	2.39	1.45	1.91	4.1
A12.6	80.01	190.78	266	4	1.31	0.75	1.51	4.5
A12.7	76.17	188.29	266	8	2.39	1.48	1.48	3.3
A12.8	76.17	191.06	266	4	1.20	0.80	1.49	2.3
A12.9	74.73	187.48	−4	8	2.46	1.48	1.49	3.1
A12.10	72.21	187.48	−4	4	1.27	0.86	1.48	3.3
A12.11	74.19	183.39	−3	8	2.37	1.51	1.51	2.9
A12.12	71.96	183.64	−3	4	1.17	0.80	1.51	3.1
A12.13	75.92	180.87	87	4	1.17	0.80	1.97	2.9
A13.1	51.49	63.60	−73	10	2.59	1.67	1.59	2.8
A13.2	50.93	65.23	108	2	0.84	0.47	1.49	4.9
A14.1	412.85	187.60	−44	12	2.94	2.43	NA	2.1
A14.2	425.81	179.25	136	10	2.94	NA	NA	—
A14.3	397.18	158.88	45	6	2.94	NA	NA	—
A15.1	425.07	194.92	35	NA	1.51	0.48	1.13	4.5
A15.2	425.07	194.92	125	NA	2.45	NA	NA	—
A16.1	450.27	186.03	237	4	1.25	0.51	0.58	4.9
A16.2	448.01	183.26	−101	6	1.26	1.10	0.92	4.3
A16.3	444.17	182.32	169	10	2.56	1.25	0.00	3.4
A17.1	409.14	209.04	59	12	4.70	2.73	2.23	7.0
A17.2	415.24	204.80	59	16	4.70	2.88	2.10	2.8
A17.3	421.72	200.05	58	16	4.70	3.12	1.70	3.0
A17.4	425.27	200.97	148	16	4.80	2.85	1.20	3.6
A17.5	427.00	199.52	148	4	1.07	0.70	NA	3.4
A18.1	404.65	206.40	202	16	4.10	1.60	2.60	5.0
A19.1	449.48	181.00	−38	8	2.40	1.45	1.45	5.8
A19.2	452.12	183.92	−83	12	3.28	2.13	1.06	4.5
A19.3	457.12	183.79	235	12	3.29	2.02	NA	7.0
A19.4	458.06	186.16	235	4	1.35	0.99	0.92	4.5
A19.5	460.05	180.21	186	12	3.12	1.96	NA	4.0

Arch damage grade (ADG).
(Continued next page.)

Table 1 (continued)
Code Name, Location, Size, and Damage Grade for Arches at the Kalat Nimrod Fortress

Code	Location X	Location Y	Azimuth	Number of Voissoirs	Span (m)	Rise (m)	Pier Height (m)	ADG
A20.1	346.20	194.67	115	8	1.77	1.16	1.22	3.6
A20.2	347.29	192.25	−65	8	1.88	1.08	1.40	4.1
GT1	40.79	140.84	−94	10	3.14	2.02	2.50	4.5
GT2	40.79	141.81	−94	8	2.15	1.50	1.35	5.5
GT3	41.00	143.05	86	8	2.15	1.42	1.30	5.4
GT9	49.00	135.36	176	6	2.71	1.73	3.29	4.4
GT10	50.83	135.33	176	2	1.37	0.93	2.10	3.9

Arch damage grade (ADG).

and lower staircase with a corridor that connects both. North of the corridor at the start of the lower staircase the passage makes a 55° turn to the east followed by a second turn of 35°, so that 90° are reached in total (Fig. 10). The latter includes two loopholes, and at the upper part of the lower staircase there are two small illumination windows. The west wall and the north wall of the tower served as the passage's outer walls, whereas the inner walls were built against the bare rock (Hartal, 2001). Both walls and the roofing barrel vault were built from large ashlars, the latter of about 0.6 × 1.2 − 1.6 m. The vault is made of two rows of these large ashlars on each side with a much smaller keystone (bottom width 0.2 m) in the middle.

From an archaeoseismological perspective, this secret passageway is of particular interest and shows an extraordinary damage pattern. The complete row of ashlars east of the keystone moved vertically down by up to 0.25 m along the upper staircase and the corridor (Fig. 10). This deformation continues beyond the corridor around both bends of the passage where it gradually decreases toward the lower end of the passageway at the postern. Figure 10c shows four crosscuts through the laser scan model of the secret passageway. We used the virtual model to measure the resulting block movement (vector sum of horizontal and vertical displacement) at sections separated by 1 m distance (Fig. 10d). The first section was taken immediately at the beginning of the remaining roof of the passageway. The large displacement here of almost 0.20 m is influenced by the missing buttresses, particularly at the western side. From section 2 to 6, which is past the first loophole, the deformation increases

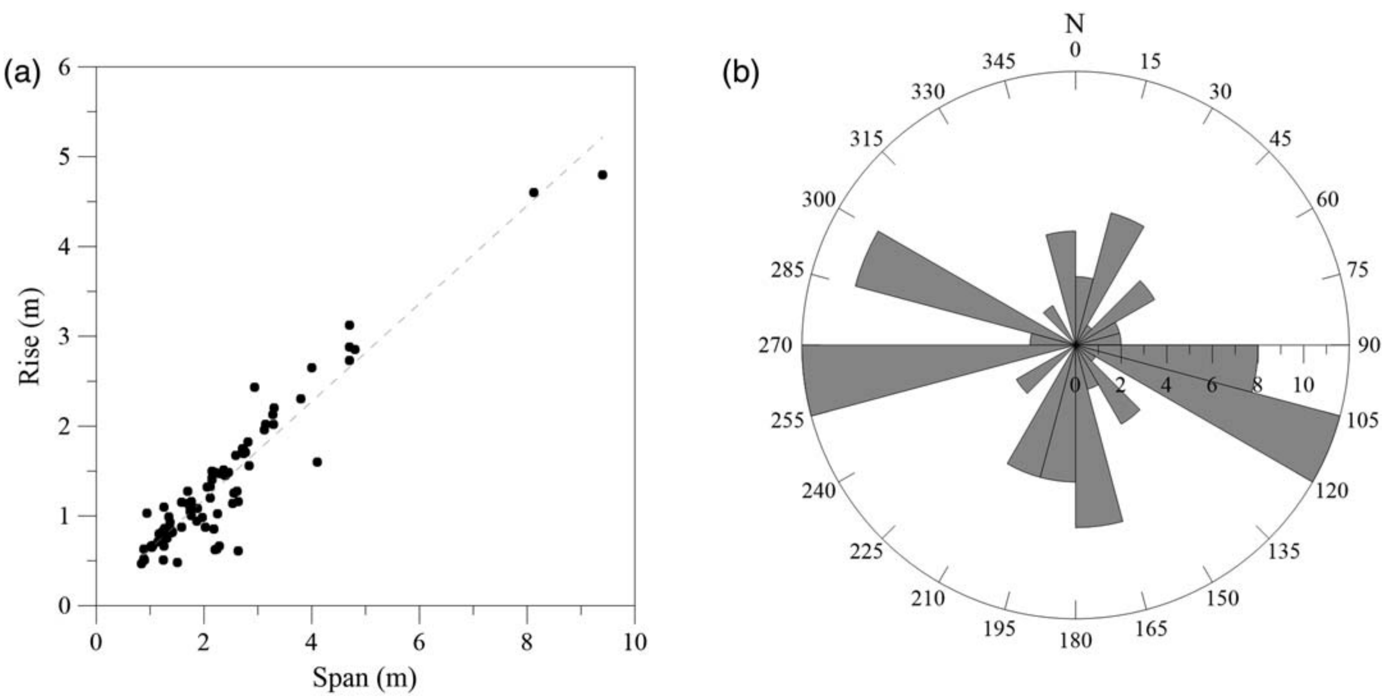

▲ **Figure 7.** (a) Measured rise of 95 arches of the Kalat Nimrod fortress with respect to the span. The dashed line is a linear regression of the data points with a slope of 0.55. (b) Rose diagram of the orientations of the 95 arches from Table 1 with respect to north; bin size is 15°.

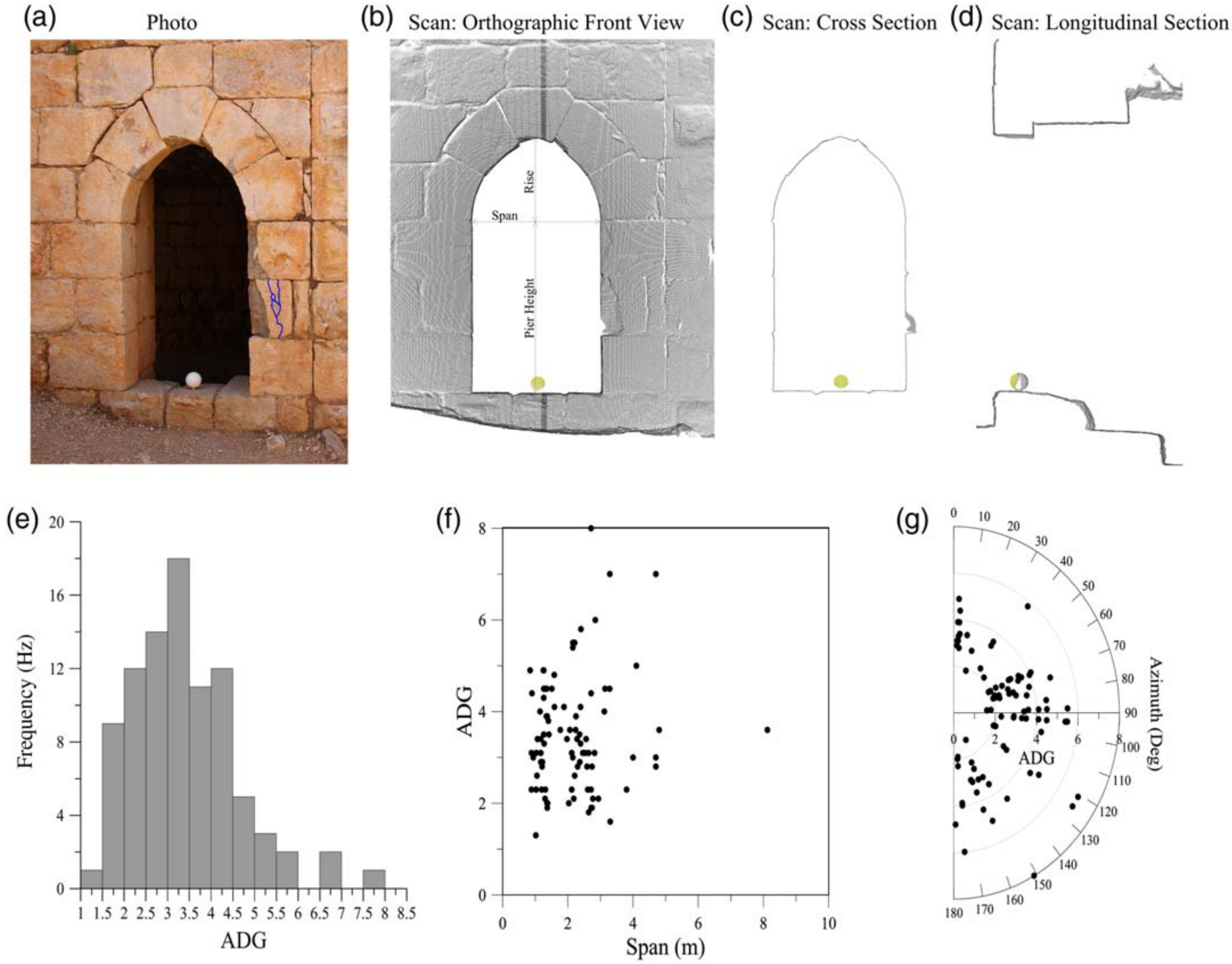

▲ **Figure 8.** Graphs used to evaluate the damage of individual arches of the Kalat Nimrod fortress and results of that evaluation. From left to right (top row) these include (a) a digital photo image (cracks are emphasized by lines, breakouts are hatched), (b) an orthographic view of the front with the main dimensions, (c) a crosscut section, and (d) a longitudinal section. All graphs are plotted to the same scale. Example is arch A1.2 in Table 1. Bottom row: (e) Histogram of the frequency of occurrence of ADGs among the 90 evaluated arches of Kalat Nimrod. Bin size is 0.5 ADG degrees. Distribution of ADGs with the (f) size (span) of arches and (g) azimuth of the arches' orientation. The color version of this figure is available only in the electronic edition.

steadily from 0.05 to 0.17 m. The following three sections (8–10), which are in the range of the second loophole, are slightly less deformed. Along the further trend of the corridor, the deformation increases toward its maximum at section 14 with a value of 0.25 m. From there we see an almost linear decrease of the deformation along the second staircase up to section 20 m just in front of the second bend of the passageway. Here, the deformation is down to 0.05 m and it vanishes at section 25. This deformation pattern cannot be evaluated by the proposed scheme from Figure 4. However, the displacements of the voussoir alone result in AGDs of 6.

The uniform drop of the first voussoir east of the keystone along the whole passageway is exactly the same deformation pattern as seen in arches GT1, GT2, and GT3, which are located east of the passage with a cross section parallel to that of the corridor. The displacement of voussoirs here is between 0.17 and 0.37 m. Figure 11 shows a damage scenario which might explain the reason for the existing deformation. The sliding voussoirs indicate a strong westerly directed component of ground motion (arrows not to scale), which disturbed the static equilibrium of the arches. The whole mass of the tower moved westward, probably with increasing amplitudes toward its top. The arches opened and allowed the voussoirs to drop before the back swing of the motion closed the gap. The ground motion also induced some corner expulsion of building material at the northwestern corner of the gate tower, which in turn was

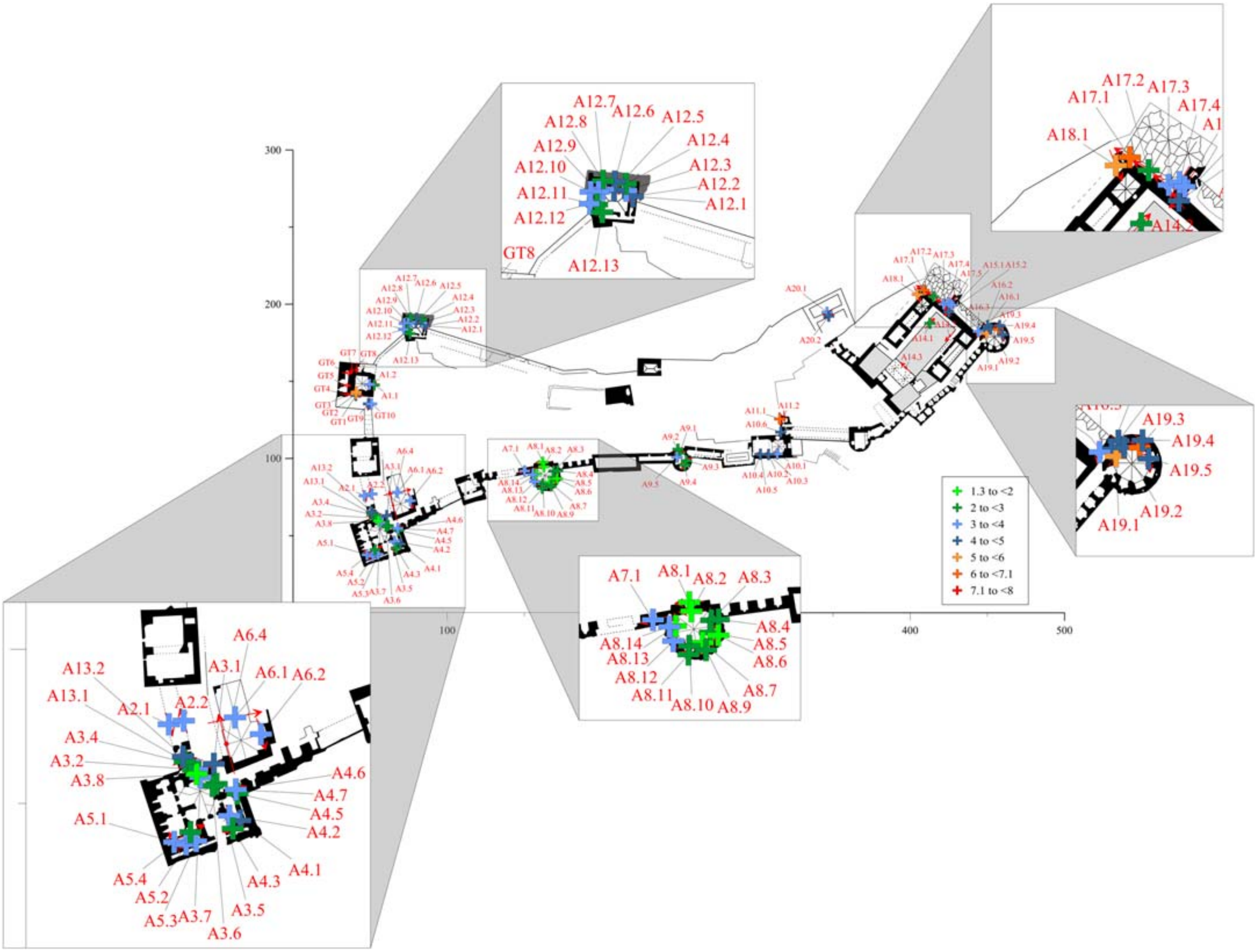

▲ **Figure 9.** On top of the map from Figure 5 the ADGs of all 90 evaluated arches are plotted. The range of values is indicated by the legend. Five zoom windows give an enlarged view of sections with dense arch coverage. At towers with arches A12.x and A8.x higher ADGs are found on the western side of the structures. For the huge tower with the arches A19.x at the northeastern corner of the fortification, the damage at the outer edge of the tower is greater than at the hill side. At the large rectangular tower at the southwestern corner, no pattern in the distribution of the damage degree was found. The color version of this figure is available only in the electronic edition.

responsible for the continuation of the voussoir sliding at the lower staircase. The motion was strong enough to topple the outer section of the gate tower, leaving an almost 45° west-dipping slope of the ruin. This rather strong directional motion also explains why Kamai and Hatzor (2007) were able to model the voussoir drop of the arch GT1 (Table 1, Fig. 6) in an east–west directed 2D discrete element model.

DISCUSSION

The ADGs defined in the selected scheme are nothing more (but also nothing less) than a systematic grading of the degree of damage of a common structural building element found in numerous excavated or persisting monuments. However, they should not be equated to site intensities.

The suggested scheme contains arbitrary and/or subjective elements (categorizing the deformation in fractions of the structure's size, small versus extended fractures, small or large spalled patches of rock, and the speculative quantity definitions); however, these factors also apply for any macroseismic scale and have proven their usefulness in a multitude of applications since their introduction by pioneers such as, for example, Mallet (1862), Mercalli (1902), and Sieberg (1904).

Although in our approach we used laser scan technology to precisely measure deformations, fracture length, spall patches, and rotations, these features can also be mapped on site with classical tools, can be taken from archaeological drawings, or can be measured on high-quality photographs. Even older black-and-white photographs of arches in archaeo-

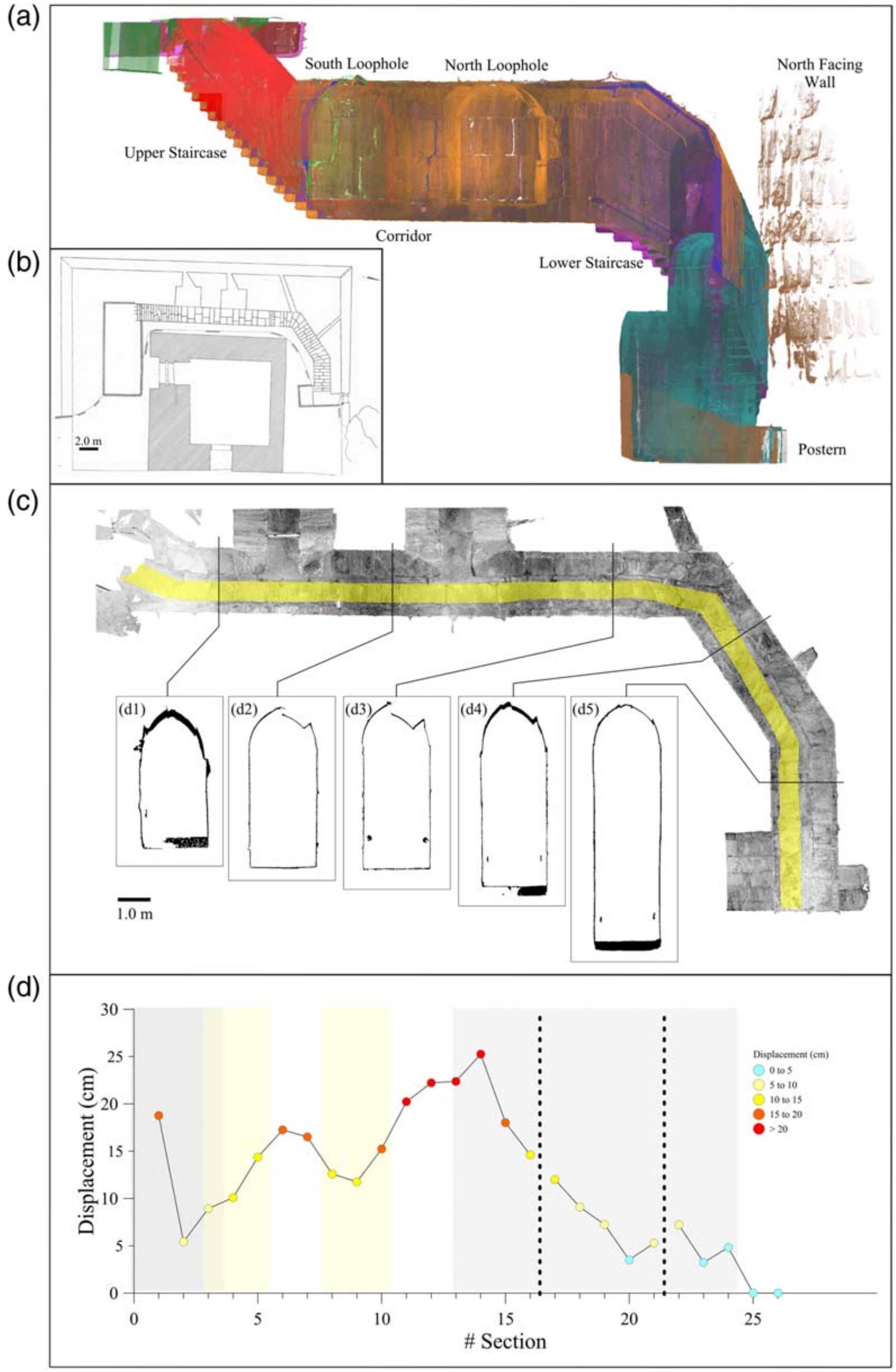

▲ **Figure 10.** (a) Perspective view from east toward the laser scan model of the secret passageway of the gate tower of Kalat Nimrod castle. Major parts of the passage are labeled. The intensity of points changes with the individual scans, which were combined into this single image. (b) Floor plan of the gate tower after Hartal (2001). (c) Orthographic view from above to the secret passageway. The light shaded ashlars moved downward by 0.10–0.15 m as shown by the crosscuts (d1–5). (d) Measured displacement of blocks from the section marked in panel (c). Sections start at the top and are separated by 1 m distance. The gray parts indicate the two staircases. The light stripe shows the location of the two loophole openings, and the dashed lines indicate the two bends of the passage. The color version of this figure is available only in the electronic edition.

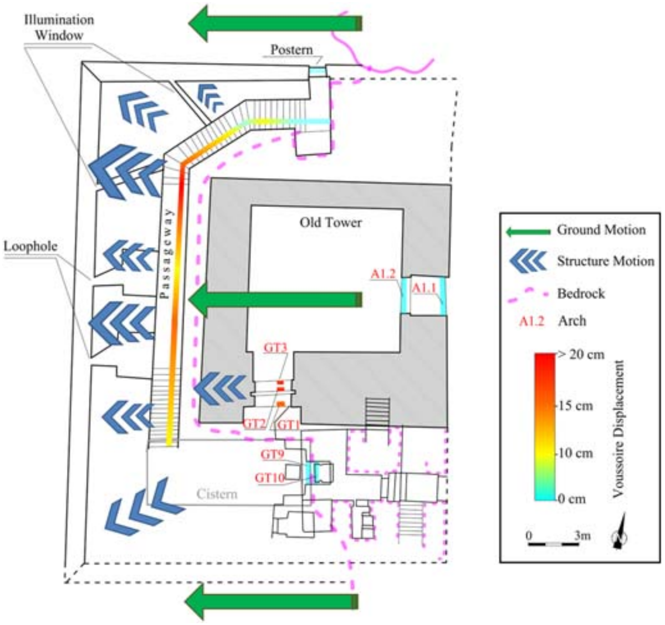

▲ **Figure 11.** Detailed plan of the gate tower (see Fig. 6). The plan shows the main features of the tower at different levels. The large arrows (not to scale) indicate the interpreted ground motion and structural reaction. The plan of the tower follows the work by Hartal (2001). The color version of this figure is available only in the electronic edition.

logical archives can be used in cases where the original arches are no longer accessible or have been altered since their discovery.

Kalat Nimrod, when struck by the 1759 Lebanon earthquake, contained many more arches than we surveyed in this study. Our selection does not represent the complete damage scenario, because we did not include in our survey the many totally collapsed arches for which the deformation of the upper part allowed the keystones to drop completely out. However, the spatial distribution of our records covers most of the site and can be considered a fairly representative sample of the arches that did not collapse.

The intention of the survey of the fortress was to test first whether the suggested evaluation scheme of ADG is of practical use and second if we can see any pattern in damage distribution throughout the large castle. The latter is not the case. When the damage grade of all surveyed arches is taken together with respect to the arches' orientations, no clear pattern can be discerned. Our original hypothesis was triggered by the obvious difference in deformation between arches GT1, GT2, and GT3 on the one hand and arches GT9 and GT10 on the other. These are located near the entrance of the inner gate in the gate tower, oriented almost exactly at 90° with respect to each other and show severe and almost no movement of voussoirs, respectively. GT9 does show severe spalling at the pillar blocks and voussoirs, also indicating a strong westerly component of ground motion. As indicated in Figure 9, this orientation-dependent voussoir movement is found throughout the gate tower including the secret passage. Although here in the gate tower the collapse obviously induced the damage of the oriented arches, this is not generally the case throughout the fortress as a whole.

The arch labeled GT1 was the object of a discrete element model by Kamai and Hatzor (2007) to estimate ground-motion parameters that caused the damage. They concluded that a peak acceleration of $1g$ at a frequency of 2 Hz within the modeled structure is sufficient to explain the deformation. This leads to a horizontal displacement of ~6 cm at the first-floor level of the tower; possibly at higher levels of the tower the displacement was even greater. These dynamic properties are in agreement with an estimate of the minimum horizontal opening that the arches GT1–3 must have experienced. Measurements from the laser scans indicate that the dislocated voussoirs required an opening of the arch between 4.5 and 5 cm.

CONCLUSION

Arches have been a common construction element to span wall openings for nearly four millennia. During earthquake ground motions they act like structural seismoscopes because a drop of keystones and/or voussoirs require a certain amount of horizontal deformation. To relate damage of arches to ground motions of an earthquake, a scheme to quantify damage grades is necessary. The scheme of ADGs introduced in this contribution showed its usefulness in evaluating damage by the 1759 Lebanon earthquake to the extended Kalat Nimrod castle. The subjective impression of a correlation between arch orientation and type and degree of damage was not confirmed by the thorough analysis of 3D laser scans and digital photographs. However, the suggested method provided a deeper insight to the damage process, particularly that of the spectacular gate tower of the castle that includes a so-called secret passage.

This approach to quantitatively evaluate damage in an archaeoseismological context—in this case, damage of arches—has shown once more that quantitative analyses are necessary in archaeoseismology to minimize subjective influence during damage interpretation.

DATA AND RESOURCES

All measures and damage features of Nimrod arches were collected as part of this study. Topography data in Figure 5 are from Shuttle Radar Topography Mission (SRTM), data available from the U.S. Geological Survey. All other data used in this article came from published sources listed in the references.

ACKNOWLEDGMENTS

We are grateful to Moshe Hartal for sharing his profound knowledge of the archaeology of Kalat Nimrod. Elisa Kagan helped with the laser scanning. Comments on an early version of the manuscript by Sharon K. Reamer helped significantly to improve the text. We thank the Israel Nature and Parks Authority and the Kalat Nimrod Park staff for the freedom to work in the park. We thank Associate Editor John Ebel for his comments and suggestions on improving the text and figures. Part of this study was funded by the German Israel Foundation (GIF) Grant Number 1165.

REFERENCES

Ambraseys, N. N. (1997). The earthquake of 1 January 1837 in southern Lebanon and northern Israel, *Ann. Geofis.* **40,** 923–935.

Ambraseys, N. N., and M. Barazangi (1989). The 1759 earthquake in the Bekaa valley: Implications for earthquake hazard assessment in the eastern Mediterranean region, *J. Geophys. Res.* **94,** 4007–4013.

Ambrose, J., and P. Tripeny (2011). *Building Structures*, John Wiley & Sons, Inc., Hoboken, New Jersey, 544 pp.

Ching, F. D. K. (2014). *Building Construction Illustrated*, Fifth Ed., Wiley & Sons, Hoboken, New Jersey, 480 pp.

Deschamps, P. (1939). *Les Châteaux des Croisés en Terre Sainte II: La défense du royaume de Jérusalem*, Paris Librairie Orientaliste Paul Geuthner (in French).

De Jong, M. J. (2012). Seismic response of stone masonry spires: Analytical modeling, *Eng. Struct.* **40,** 556–565.

De Jong, M. J., and C. Vibert (2012). Seismic response of stone masonry spires: Computational and experimental modeling, *Eng. Struct.* **40,** 566–574.

De Lorenzis, L., M. DeJong, and J. Ochsendorf (2007). Failure of masonry arches under impulse base motion, *Earthq. Eng. Struct. Dyn.* **36,** 2119–2136, DOI: 10.1002/eqe.719.

Dym, C. L., and H. E. Williams (2011). Stress and displacement estimates for arches, *J. Struct. Eng.* **49,** doi: 10.1061/(ASCE)ST.1943-541X.0000267.

Ellenblum, R. (1989). Who built Qal'at al Subayba? *Dumbarton Oaks Papers* **3,** 103–112.

Ellenblum, R., S. Marco, R. Kool, U. Davidovitch, R. Porat, and A. Agnon (2015). Archaeological reconstruction of earthquake ruptures in Tell Ateret, the Dead Sea Fault, *Tectonics* **34,** 2105–2117, doi: 10.1002/2014TC003815.

Fanning, P. J., T. E. Boothby, and B. J. Roberts (2001). Longitudinal and transverse effects in masonry arch assessment, *Construct. Build. Mater.* **15,** 51–60.

Garfunkel, Z. (1981). Internal structure of the Dead Sea leaky transform (rift) in relation to plate kinematics, *Tectonophysics* **80,** 81–108.

Garfunkel, Z. (1991). Darfur–Levant array of volcanics: A 140-Ma-long record of a hot spot beneath the African–Arabian continent, and its bearing on Africa's absolute motion, *Israel J. Earth Sci.* **40,** 135–150.

Garfunkel, Z., I. Zak, and R. Freund (1981). Active faulting in the Dead Sea rift, *Tectonophysics* **80,** 1–26.

Grünthal, G. (Editor) (1998). European Macroseismic Scale 1998, *Counceil de'l Europe, Cahiers Centre Européen Géodynamique Séismologie* **15,** 99 pp.

Gomez, F., M. Meghraoui, A. N. Darkal, R. Sbeinati, R. Darawcheh, C. Tabet, M. Khawlie, M. Charabe, K. Khair, and M. Barazangi (2001). Coseismic displacements along the Serghaya fault: An active branch of the Dead Sea Fault System in Syria and Lebanon, *J. Geol. Soc.* **158,** 405–408.

Hartal, M. (2001). *The Al-ubayba (Nimrod) Fortress: Towers 11 and 9*, Israel Antiquities Authority, Jerusalem, 3–74.

Kamai, R., and Y. H. Hatzor (2007). Numerical analysis of block displacements in ancient masonry structures: A new method to estimate historic ground motions, *Int. J. Numer. Anal. Meth. Geomech.* **32,** 1321–1340.

Mallet, R. (1862). *Great Neapolitan Earthquake of 1857: The First Principles of Observational Seismology*, Vol. 1, Royal Society London, Chapman and Hall, 431 pp.

Marco, S. (2008). Recognition of earthquake-related damage in archaeological sites: Examples from the Dead Sea fault zone, *Tectonophysics* **453,** 148–156, doi: 10.1016/j.tecto.2007.04.011.

Marco, S., A. Agnon, R. Ellenblum, A. Eidelman, U. Basson, and A. Boas (1997). 817-year-old walls offset sinistrally 2.1 m by the Dead Sea Transform, Israel, *J. Geodyn.* **24,** 11–20.

Marco, S., T. K. Rockwell, A. Heimann, U. Frieslander, and A. Agnon (2005). Late Holocene slip of the Dead Sea Transform revealed in 3D palaeoseismic trenches on the Jordan Gorge segment, *Earth Planet. Sci. Lett.* **234,** 189–205, doi: 10.1016/j.epsl.2005.01.017.

Mercalli, G. (1902). Sulle modificazioni proposte alla scala sismica De Rossi–Forel, *Boll. Soc. Sismol. Italiana* **8,** 184–191.

Nemer, T., and M. Meghraoui (2006). Evidence of coseismic ruptures along the Roum fault (Lebanon): A possible source for the AD 1837 earthquake, *J. Struct. Geol.* **28,** 1483–1495.

Nemer, T., M. Meghraoui, and K. Khair (2008). The Rachaya–Serghaya fault system (Lebanon): Evidence of coseismic ruptures, and the AD 1759 earthquake sequence, *J. Geophys. Res.* **113,** no. B5, B05312.

Robinson, G. (1837). *Travels in Palestine and Syria*, Kessinger, Whitefish, Montana, 470 pp.

Rodríguez-Pascua, M. A., R. Pérez-López, J. L. Giner-Robles, P. G. Silva, V. H. Garduño-Monroy, and K. Reicherter (2011). A comprehensive classification of earthquake archaeological effects (EAE) in archaeoseismology: Application to ancient remains of Roman and Mesoamerican cultures, *Quaternary Int.* **242,** 20–30, doi: 10.1016/j.quaint.2011.04.044.

Ron, H. (1987). Deformation along the Yamouneh, the restraining bend of the Dead Sea transform: Paleomagnetic data and kinematic implications, *Tectonics* **6,** 653–666.

Schloen, D. (1995). Recent discoveries at Ashkalon, *The Oriental Institute of the University of Chicago* **145,** 1–6.

Sieberg, A. (1932). *Erdbebengeographie, Handbuch der Geophysik*, Band IV, Borntraeger, Berlin, Germany, 527–1005 (in German).

Sieberg, A. (1904). *Handbuch der Erdbebenkunde*, F. Vieweg und Sohn, Braunschweig, Germany, 363 pp. (in German).

Sneh, A., and R. Weinberger (2003). Geology of the Metulla quadrangle, northern Israel: Implications for the offset along the Dead Sea Rift, *Israel J. Earth Sci.* **52,** 123–138.

Sneh, A., and R. Weinberger (2014). Geological map of Israel 1:50, 000 Metulla Sheet 2-II, *Geol. Surv. Israel.*

Wilson, M., A. E. Shimron, J. M. Rosenbaum, and J. Preston (2000). Early Cretaceous magmatism of Mount Hermon, Northern Israel, *Contrib. Mineral. Petrol.* **139,** 54–67.

Klaus-G. Hinzen
Iris Schwellenbach
Gregor Schweppe
Earthquake Geology and Archaeoseismology
Institute for Geology and Mineralogy
Cologne University
Erdbebenstation Bensberg
Universität zu Köln
Vinzenz-Pallotti-Str. 26
51429 Bergisch Gladbach, Germany
hinzen@uni-koeln.de
i.schwellenbach@uni-koeln.de
g.schweppe@uni-koeln.de

Shmuel Marco
Department of Geosciences
Tel Aviv University
Ramat-Aviv
Tel-Aviv 69978, Israel
shmulikm@tau.ac.il

Published Online 2 March 2016